



Performances Investigation of Ti6Al4V Alloy Modified by Plasma Nitriding + Plasma Enhanced Chemical Vapor Deposition and Laser Remelting Process in Simulated Body Fluid

Jing Zhang¹ · Kangmei Li¹ · Jun Hu¹

Received: 7 April 2020 / Accepted: 15 May 2020 / Published online: 13 June 2020
© The Korean Institute of Metals and Materials 2020

Abstract

To enhance the corrosion and wear resistance of biological titanium alloy Ti6Al4V in the human body, plasma nitriding + plasma enhanced chemical vapor deposition (PN + PECVD), laser remelting (LR) process were employed to modify the titanium alloy, respectively. The microhardness of LR and PN + PECVD samples was reported to increase by 117% and 165%, respectively, in contrast to that before the samples were modified. The thickness of LR modified layer was reported as 10 μm , and the nitrided film on the surface of PN + PECVD sample exhibited the thickness of 2 μm . The wear and corrosion performances of three samples were analyzed by friction and corrosion experiments in the simulated body fluid. As revealed from the experimental results, the wear rates of LR and PN + PECVD samples were 74.1% and 94.5% lower than that of Ti6Al4V. It can be seen that the surface modification layer can play a good role in protecting Ti6Al4V substrate from wear. By the electrochemical corrosion experiment, the corrosion resistance of Ti6Al4V, LR and PN + PECVD samples was ranked as PN + PECVD > LR > Ti6Al4V. It is therefore speculated that the PN + PECVD and LR modification processes could noticeably enhance the corrosion and wear resistance of Ti6Al4V in the human body.

Keywords Titanium alloy · PECVD · Laser remelting · Wear · Corrosion · Simulated body fluid

1 Introduction

Titanium and its alloys are the major materials for human orthopedic implants for their high biocompatibility, low elastic modulus and prominent mechanical properties [1]. Nevertheless, titanium alloy exhibits low hardness and poor wear resistance; it is hard to form an oxidation film quickly when worn in human body fluid [2]. Thus, the internal substrate is exposed to human body fluid, thereby increasing the abrasion. The wear debris and corrosion products generated by abrasion or corrosion process will penetrate into organic tissues, accumulate in several organs, and even access to the whole circulation system, which can cause a range of degrees of physiological response or cause tissue structure to vary [3, 4]. Accordingly, the surface of titanium alloy implants should be modified to enhance its wear and

corrosion resistance in human body. It is an effective method to enhance the corrosion and wear resistance of titanium alloy by producing an oxidation film or a nitride film on the surface of titanium alloy through the modification process [5].

PECVD refers to a method of producing corrosion-resistant and wear-resistant films on the metal surface. It is determined by the electron in plasma to activate the chemical reaction of vapor deposition, i.e., to down-regulate the internal stress attributed to the mismatch of the film and substrate expansion coefficient, as well as to enhance the deposition rate [6–9]. Mina et al. [10] explored the preparation of nano-TiC_{0.3}N_{0.7} coating into tool steel with PACVD technology. The hardness of the coating was enhanced, and such coating exhibited good wear resistance and prominent mechanical properties. Hamed et al. [11] adopted PACVD to deposit Ta-based films to enhance the biological corrosion behavior of AISI316L stainless steel. Ta/TaN films exhibit higher integrity than single-layer Ta films and stronger binding force with substrate; both of them display excellent corrosion resistance and biocompatibility. Though PECVD or PACVD can effectively deposit high-performance films on the substrate surface, the deposited

✉ Jun Hu
hjmorning@hotmail.com

¹ School of Mechanical Engineering, Donghua University, Shanghai 201620, China

films still have defects (e.g., large hardness gradient between the surface hardness and the substrate hardness, as well as unstable bonding strength with the substrate) [12–14].

Plasma nitriding treatment refers to a process that complies with glow discharge principle, adopts the test piece as cathode into a negative pressure vessel filled with nitrogen, and subsequently electrifies the nitrogen and hydrogen atoms to be ionized, as to form a plasma area between the anode and cathode. Under the robust electric field in the plasma region, the positive ions of nitrogen and hydrogen will bombard the surface of the workpiece at high speed. The high kinetic energy exhibited by the ions is converted into heat energy, and the specimen surface is heated to the required temperature. As impacted by the bombardment of ions, the surface of the workpiece is sputtered with atoms, so it gets purified. In the meantime, for the adsorption and diffusion, the nitrogen element penetrates into the surface of the workpiece, thereby forming compounds, which aims to enhance the corrosion and wear resistance of the material [15, 16]. Sun et al. [17] performed the mechanical grinding and plasma nitridation on the surface of pure titanium; they reported that the mechanical properties of pure titanium were enhanced. In vitro cell experiments, it was reported that the cells on the surface of the modified samples were value-added and differentiated. Based on plasma nitrogen treatment chromium coating, Zhang et al. [18] studied the effect of microstructure and nano-mechanical properties of aluminum alloy. As proved experimentally, the surface hardness and wear resistance of aluminum alloy were enhanced after the sample was examined. Though plasma nitriding treatment could enhance the surface hardness of metal implants, the thin nitriding film formed on the surface of plasma nitrogen treatment and the uneven composition of the film affected the wear and corrosion resistance of titanium alloy [19]. For the limitations of PECVD and plasma nitrogen treatment, the plasma nitrogen + plasma enhanced chemical vapor deposition (PN+PECVD) process was adopted in the present study to modify Ti6Al4V titanium alloy. Such process was a plasma composite process, with PECVD performed continuously after surface nitrogen treatment. Furthermore, Ti6Al4V samples were modified by laser remelting (LR), and the effects of the two processes on the corrosion and wear properties of Ti6Al4V in the simulated body fluid were delved into and compared, experimentally and theoretically underpinning the surface modification and strengthening technology of biological titanium alloy implants.

2 Material and Method

2.1 Titanium Alloy Sample

Medical Ti6Al4V alloy, purchase from Shanghai Chun-Ming Metal Material Co., Ltd., was adopted as the

substrate material, with the sample size of $15 \times 15 \times 5$ mm and the chemical composition (wt%): Ti 88.94, Al 5.7, V 4.26, C 0.89, Fe 0.21. The Ti6Al4V sample was sanded with 400 #, 800 #, and 1200 # sandpaper, respectively, and then mechanically polished with the alumina polishing solution to smooth the surface. Subsequently, the sample was washed with alcohol to get dried naturally.

2.2 Laser Remelting (LR)

The laser remelting modification process adopted RFL-A2000D type fiber laser system, which rated output power is 2000 W. The Ti6Al4V alloy was remelted under the laser power of 400 W, the distance from the light exit to the sample as 100 mm, the spot diameter of 5 mm, and at the laser scanning speed of 3 m/min. Samples cooled naturally after remelting.

2.3 Plasma Nitrogen + Plasma Enhanced Chemical Vapor Deposition (PN + PECVD)

PN + PECVD modifying processes were performed with the LHJMY50A-2 type plasma nitrogen treatment process equipment. The process flow chart is given in Fig. 1. The characteristic of the process is that the surface nitrogen treatment of plasma material was performed first, and then PECVD was conducted in nitrogen treatment furnace, which is a novel composite process of plasma nitrogen treatment and plasma enhanced chemical vapor deposition process promoted. The nitrogen treatment strengthening layer on the Ti6Al4V and nitriding film on the surface could be well combined.

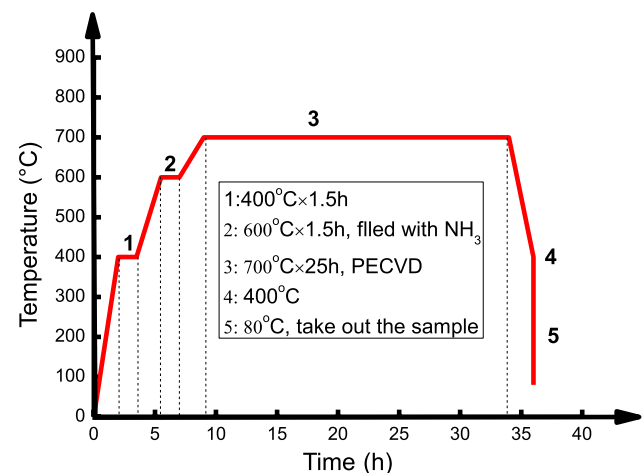


Fig. 1 PN+PECVD composite process flow chart

2.4 Morphology and Phase

The surface-interface morphology and elements of Ti6Al4V, LR and PN + PECVD samples were analyzed with a ZEISS EVO18 type SEM as well as its EDS. The phases were studied using a D/max2500 PC type X-ray diffractometer.

2.5 Microhardness

HVS-1000 M type microhardness tester was employed to ascertain the surface microhardness and the hardness gradient of the interfaces of Ti6Al4V, LR and PN + PECVD samples. Before the hardness test was performed, the sample was wiped with alcohol to remove the stains on the samples surface. The experimental stress load of microhardness tester reached 10 N, and the stress holding time was set to 10 s. The hardness value was calculated using the microhardness tester system automatically.

2.6 Friction and Wear Test

The friction-wear test was performed on a CFT-I type reciprocating friction-wear tester based on ball-plane sliding contact. The grinding ball was Si₃N₄ ceramic ball, exhibiting the diameter of Ø5 mm, wear length of 5 mm, test time of 30 min, load of 8 N, as well as the reciprocating frequency of 200t/min. This study performed the friction-wear test in SBF. The composition of SBF is NaCl 8.69 g/L, KCl 0.30 g/L, CaCl₂ 0.48 g/L, and the pH of the solution was set to 7.4. After the experiment, the wear scar morphology was characterized by SEM and EDS.

2.7 Electrochemical Corrosion Test

Electrochemical experiments were performed in the CHI660 electrochemical workstation. After being cleaned and dried, Ti6Al4V, LR and PN + PECVD surface that did not need to be tested were sealed with resin. In order to simulate the human body conditions, the SBF were used as the test electrolytes and the tests were carried out at 37 ± 1 °C. A platinum sheet as the counter electrode and a saturated calomel (SCE) as the reference electrode were used. The surface of samples was cleaned by deionized water and acetone. The test surface area of the sample was fixed at 2 cm², and the rest of the area except the exposed area was wrapped with a strong polymer adhesive to prevent crevice corrosion. After the experiment, CHI 660 electrochemical workstation system could automatically plot the fitting Tafel curve. Tafel curves were obtained within the potential range from -0.4 VSCE to 0.4 VSCE with a scan rate of 1 mV/s.

3 Results and Discussion

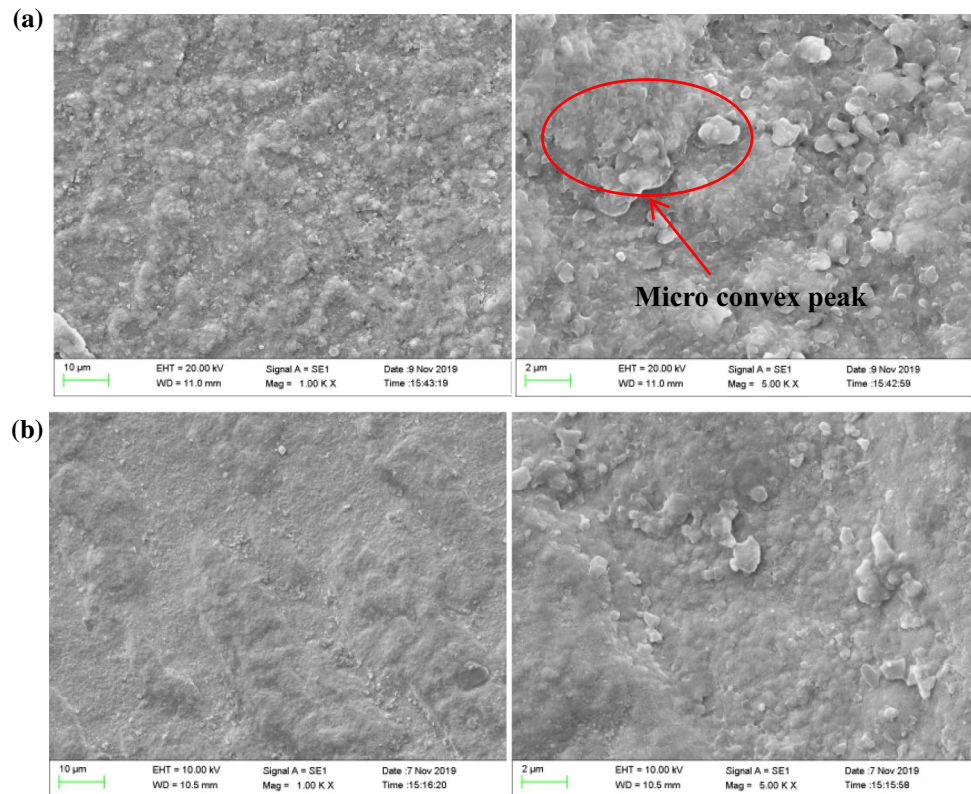
3.1 Micromorphology Analysis

After laser remelting was performed, the chemical composition on the surface of titanium alloy included (mass%) Ti 79.37, O 8.74, Al 4.37, V 4.80, C 2.42, as well as Fe 0.03. Because the boiling point of solid Al is much lower than that of Ti, under laser radiation, a small amount of Al was vaporized due to high temperature, which caused the Al content in the remelted layer to decrease. Figure 2a presents the surface morphology of LR sample. LR sample had an uneven surface, belonging to the typical laser melting morphology, of which the morphology under the high magnification is illustrated in Fig. 2a. It is suggested that a small amount of warped metal particles adhered to LR sample surface, and stacking phenomenon existed, thereby resulting in the enhancement of the surface roughness of LR sample. However, as impacted by the reasonable control of laser power, cracks and over-burning phenomenon did not appear on the surface modified layer, and the surface was relatively not damaged.

After PN + PECVD treatment, the chemical composition on the surface of Ti6Al4V reached (mass%): Ti 77.20, Al 5.95, N 7.43, V 4.71, C 2.02, O 2.65, Fe 0.01. Figure 2b give the surface morphology. A small amount of slight convexity appeared on the surface of titanium alloy, and its roughness was enhanced compared with that before PN + PECVD. PECVD process refers to a chemical reaction in which the kinetic energy of the electrons in the plasma activated the gas phase, namely, the chemically active ions and radicals were generated, reacting with other ions, atoms and molecules in the gas phase, or causing lattice damage and chemical reaction on the material substrate surface. The reaction gas in the plasma body dissociated for the collision of high-energy electrons. As impacted by the electric field strength, gas pressure, etc., and the electrons could not act on the TiN film surface to be absolutely uniform, resulting in the enhancement of the surface roughness of the nitride film [20].

Figure 3 illustrates the interface morphology and element scanning of titanium alloy after LR. Figure 3a shows the melting interface of LR sample at low and high magnification, respectively. It suggests that the average depth of the melting layer was nearly 10 µm. To analyze the mechanism of laser remelting on the strengthening of titanium alloy surface, the element scanning was performed on the interface after laser remelting, as described in Fig. 3b. The content of Ti, Al, V and other elements in the melting zone were lower than those in the titanium alloy substrate, while O content was elevated in the melting zone. According to the scanning of the Ti and O elements in Fig. 3c shows that

Fig. 2 **a** Surface morphology of LR sample low-magnification, **b** surface morphology of PN+PECVD sample



the distribution trends of Ti and O elements in the melting zone were similar. To be specific, during laser remelting, the high temperature made the titanium alloy substrate react with O element in the air to form titanium oxides. The formation mechanism of these compounds would be delved into based on XRD results.

The interface morphology and element scanning of titanium alloy treated by PN+PECVD process is presented in Fig. 4. Figure 4a gives the morphology of the interface at low and high magnification, respectively. It is shown that a layer of TiN deposition film was formed with a thickness of 2–3 μm on the surface of titanium alloy, and the nitrided layer deposited evenly on the surface of titanium alloy, without any bubble and pore, while the boundary was tightly combined with the substrate. The element line scanning was performed at the position of Fig. 4b and the scanning results are given in it, in which Ti element exhibited a lower content distribution on the surface, while a higher content of N element was achieved on the Ti6Al4V surface. Furthermore, a slow decreasing trend from the surface to the interior was presented, rather than a sudden decrease of elements. The scanning results of Ti and N elements are presented in Fig. 4c. Ti elements were scarcely gathered on the surface. The distribution of N elements in the substrate did not noticeably differ from that on the surface, demonstrating that in the process of heat preservation, chemical vapor deposition could effectively combine the deposition layer

with the substrate and lower the N content gradient between the deposition layer and the substrate.

3.2 XRD Analysis

Figure 5 presents the XRD diffraction analysis curve of Ti6Al4V, LR and PN+PECVD samples. Figure 5a reveals that the major diffraction peak of titanium alloy substrate was Ti. Figure 5b gives the analyzed results of the phase on the surface of titanium alloy after LR. The diffraction peaks of TiO_2 , TiO and Ti_6O were suggested on the surface of titanium alloy, associated with the process of laser remelting. Titanium reacted rapidly with oxygen in the air, while oxygen accessed into the lattice of titanium surface. In the meantime, the solid solution reaction of oxygen in titanium substrate was slower than oxidation reaction, and the solid solution oxygen could be neglected. The oxidation reaction led to the formation of a compact oxide film on titanium surface. At the temperature lower than 500 $^\circ\text{C}$, the oxidation film on the surface could prevent oxygen from diffusing to the interior and being oxidized. During laser processing, with the rise in temperature, the oxidation film on the surface began to dissolve, and oxygen accessed into the inner lattice of metal. At the temperature over 700 $^\circ\text{C}$, oxygen was promoted to diffuse to the metal. In the meantime, the TiO oxide layer was formed between the surface TiO_2 and the substrate, while the oxidation film became sparse, and its

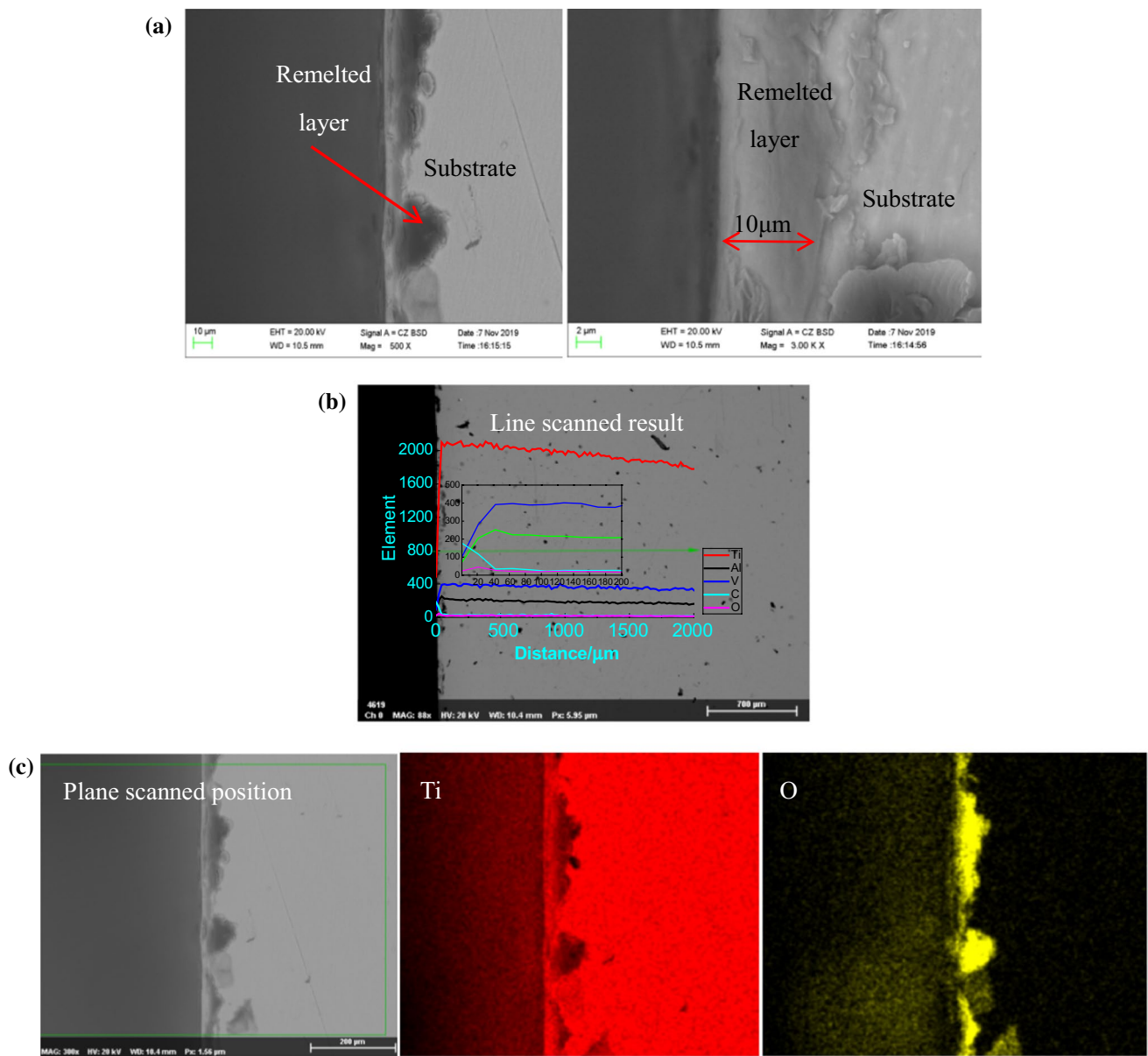
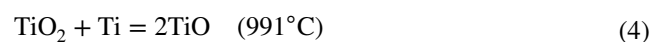
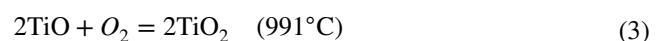
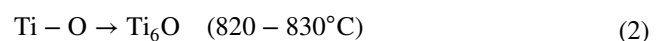
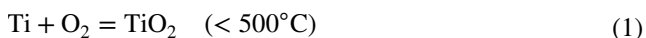


Fig. 3 **a** Cross-section morphology of LR sample, **b** element line scanned analysis of LR sample, **c** element plane scanned analysis of LR sample

protective function was lost. At the temperature of 820 °C, TiO would be converted into Ti_6O . At the temperature over 950 °C, the oxidation reaction between titanium and oxygen in the air turned more intense. The oxygen in the oxidation film diffused into the substrate via the anion vacancy and the phase boundary of different oxides, while titanium diffused to the surface, thereby intensifying the oxidation reaction process. The specific reaction equations are expressed in formula (1)–(4) [21–23]:



Since there were various stable oxides in Ti–O system, the composition of the film formed by titanium at high temperature was relatively complicated, and the density of the film decreased gradually from low-valence oxides to high-valence oxides. With the rise in heating temperature,

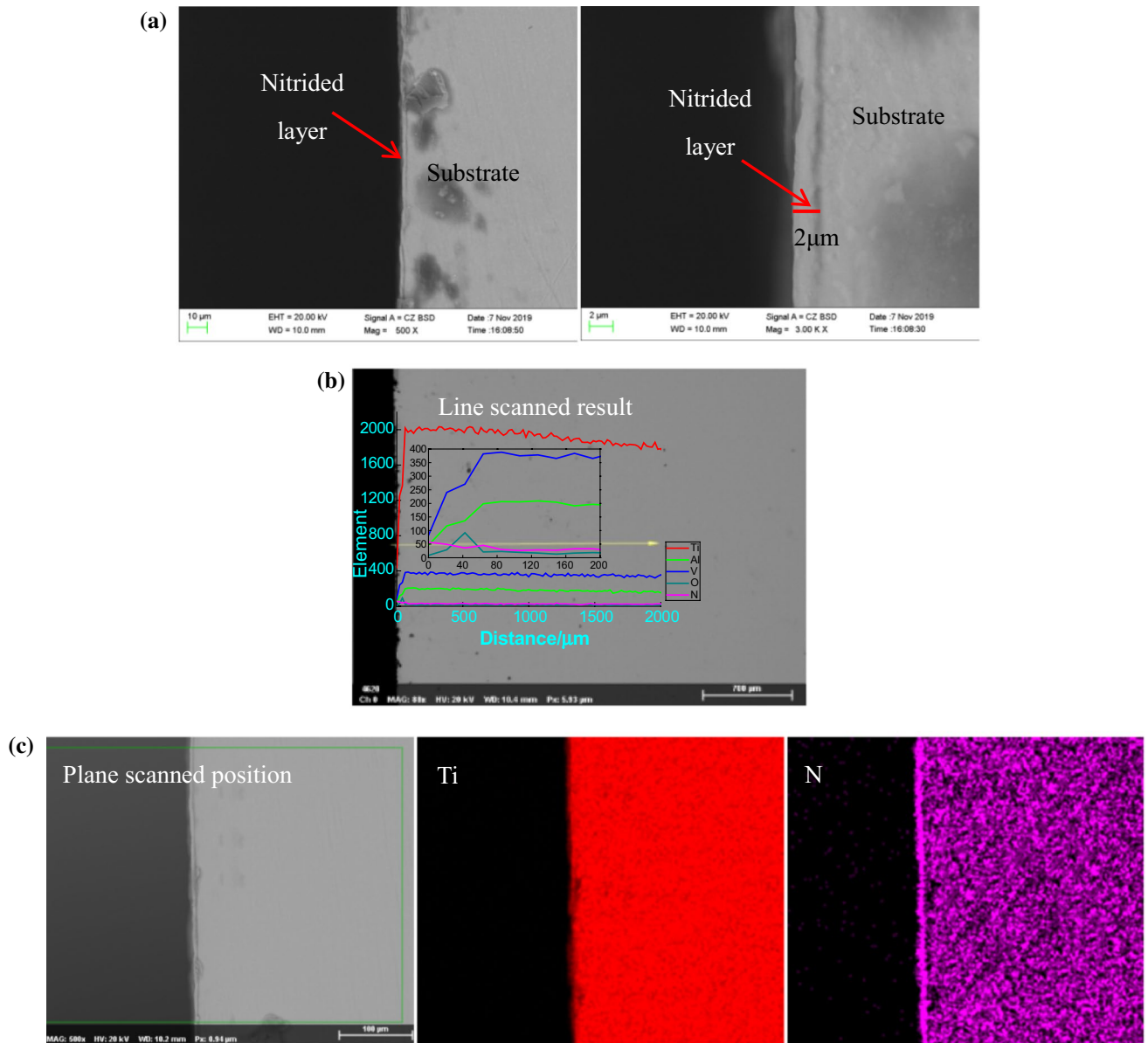


Fig. 4 **a** Cross-section morphology of PN+PECVD sample, **b** element line scanned analysis of PN+PECVD sample, **c** element plane scanned analysis of PN+PECVD sample

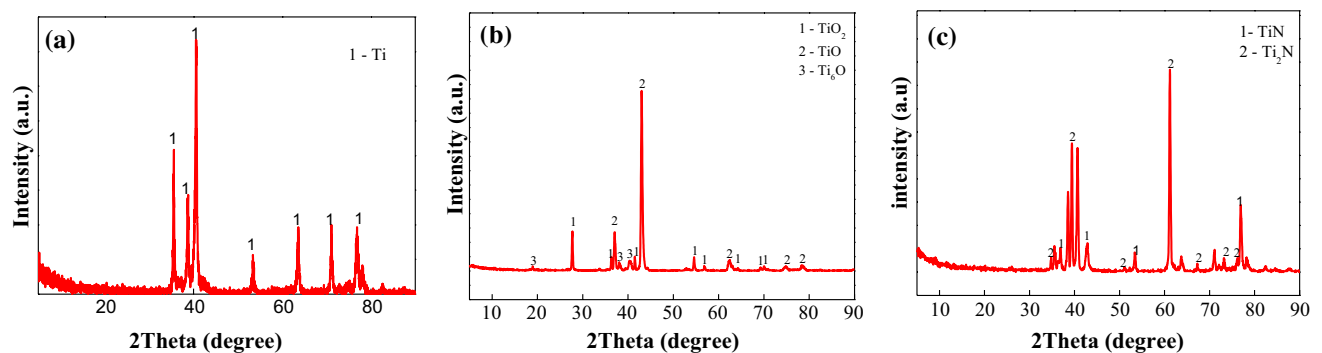


Fig. 5 XRD analyses **a** Ti6Al4V, **b** LR sample, **c** PN+PECVD sample

the solubility of oxygen in titanium was elevated. At the same time, the saturation degree of oxygen in the oxide declined, leading to the reduction reaction to dioxide and the formation of low-valence oxide. The density of surface oxide increased, and the specific volume decreased, which was the underlying cause of the formation of various Ti–O-based compounds at different temperatures.

Figure 5c shows the phase analysis curve of titanium alloy surface after PN + PECVD processing. Diffraction peaks of TiN and Ti₂N are suggested on the surface of titanium alloy after modification. The deposition film of PECVD primarily consisted of TiN (δ). TiN (δ) phase exhibited good wear resistance, whereas the formation of TiN (δ) during the plasma nitrogen treatment was often accompanied by the formation of Ti₂N (ε) [17]. Taktak et al. analyzed the diffusion mechanism of Ti–N compound by temperature during plasma nitrogen treatment; they reported that the phase composition of nitriding layer was tightly associated with its nitriding temperature. The Ti–N phase formed by plasma nitrogen treatment substantially refers to multi-phase diffusion process, in which the growth of each layer was regulated by the chemical diffusion rate and interface flux in the layer. At 700 °C, the diffusion coefficient of TiN reached 2.66×10^{-12} , while the diffusion coefficient of Ti₂N was 2.17×10^{-11} , and α-Ti did not diffuse [24].

Furthermore, for the mutual diffusion of Ti–N-based compounds formed in plasma nitrogen treatment in the substrate and the film deposited by the vapor deposition, the Ti₂N (ε) phase appeared on the deposited film surface. Such diffusion was conducive to facilitating the

combination of the chemical vapor deposition film and the substrate.

3.3 Hardness and Hardness Gradient

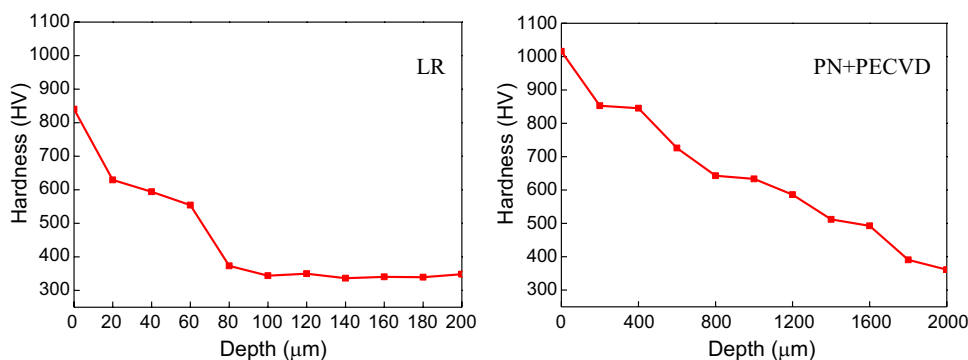
The microhardness of the titanium alloy substrate surface and the two types of modified Ti6Al4V are listed in Table 1. The microhardness of LR sample was enhanced by 117%, higher than that of the titanium alloy substrate. For the temperature gradient produced by laser remelting treatment on the surface of titanium alloy, the surface grains were refined. Moreover, the compounds of Ti–O series generated in the remelting process exhibited higher hardness. After PN + PECVD, the hardness of the samples was enhanced by 165%. With the composite process of PN + PECVD, a dense Ti–N film was formed on the surface of Ti6Al4V, exhibiting a higher hardness.

The microhardness distribution of the interface of the two modified samples is illustrated in Fig. 6. It reveals that the microhardness of sample after laser remelting declined from the remelting face to the substrate, which complied with the hardness of the Ti6Al4V at the depth of nearly 70 μm. A layer 0–5 μm at the interface could be considered the laser remelting area, and 5–70 μm refers to the heat affected area. After PN + PECVD treatment, the microhardness of the samples at the interface varied moderately without big hardness gradient. At the depth of approximately 1.8 mm, the hardness value was lowered to the hardness of the substrate, suggesting that the depth of the nitriding was about 1.8 mm.

Table 1 Microhardness of surface

Sample	Microhardness/HV					Average/HV
	Point 1	Point 2	Point 3	Point 4	Point 5	
Ti6Al4V	374.63	349.43	414.59	388.05	406.61	386.66
LR sample	788.77	829.59	842.91	863.52	876.31	840.33
PN + PECVD sample	1039.40	970.00	953.61	1027.43	1131.60	1024.41

Fig. 6 Mic-hardness of cross-section



3.4 Friction and Wear Performance Analysis

After friction and wear test, the friction coefficients of the three samples are given in Fig. 7a. The average friction coefficients of Ti6Al4V, LR and PN reached 0.658, 0.615 and 0.478, respectively, while the standard deviation of the friction coefficient were 0.091, 0.05 and 0.022, respectively. As revealed from the Fig. 7 and calculation results, the friction coefficient of the sample treated by the PN + PECVD treatment was the minimal, and the fluctuation was the smallest, followed by laser remelting sample, and the Ti6Al4V was the worst; this finding displayed direct relations to the surface hardness of the three samples. Ti6Al4V exhibits low hardness, making it easy to produce adhesion with ceramic grinding ball, and the achieved friction coefficient and the fluctuation gradient were large. After LR, the fluctuation range of friction coefficient was narrowed, whereas the value of friction coefficient varied irregularly in range of time areas. This results was because laser remelting could cause the rise in surface roughness of titanium alloy, the

radial force of the grinding ball was up-regulated when the micro convex peak of the surface, and the grinding ball were grinded against each other, thus causing the friction coefficient to rise. Titanium alloy treated by PN + PECVD exhibited high surface hardness, the surface was relatively flat, and the friction coefficient kept stable around a certain value. The width, depth and wear rate of the worn cracks are listed in Table 2. After modification, the two samples exhibited better wear performance, and the wear rate of PN + PECVD sample was the minimal.

The micro-morphology of the worn cracks of Ti6Al4V substrate, LR sample and PN + PECVD sample under 10 N load is illustrated in Fig. 7b. There were scratches appearing along the sliding direction in the worn crack of Ti6Al4V substrate, and there was noticeable material migration phenomenon. Since the hardness of Ti6Al4V substrate material was significantly lower than Si_3N_4 ceramic ball, and the plasticity of titanium alloy was high, the oxidation film on the surface of titanium alloy fallen off and began to appear plastic deformation during the friction and wear processes.

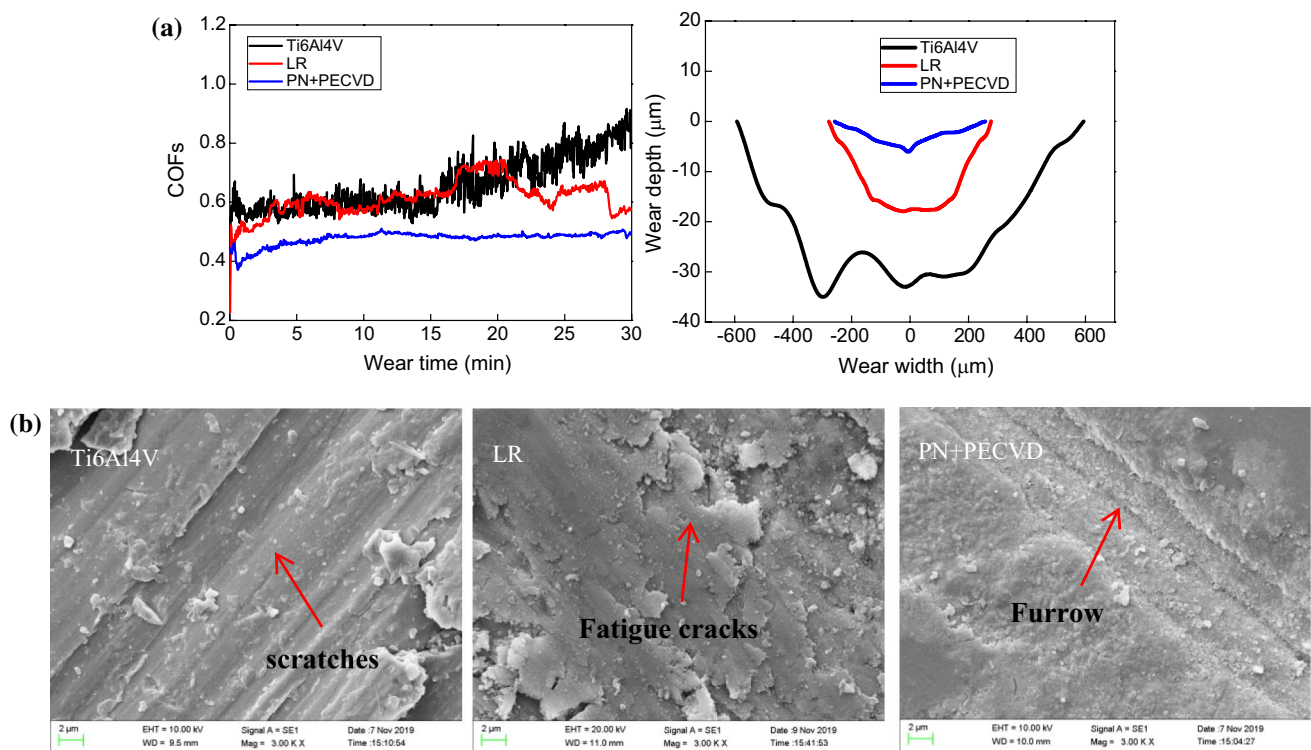


Fig. 7 a COFs vs wear time and wear profiles of Ti6Al4V, LR and PN + PECVD samples, b morphology of worn tracks

Table 2 Wear parameters

Sample	Wear width/μm	Wear depth/μm	Wear rate/mm ³ /N m
Ti6Al4V	1185.94	34.99	2.18×10^{-4}
LR sample	555.06	17.93	5.65×10^{-5}
PN + PECVD sample	515.62	6.02	1.20×10^{-5}

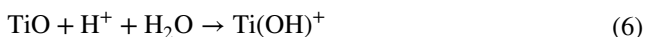
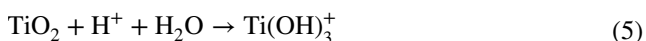
Under a large load, the metal in the worn crack migrated under the radial force, thereby forming the worn crack morphology, as shown in the figure, and the wear mechanism belonged to adhesive wear at that moment.

The worn crack of LR sample displayed a shallow pit shape, in which there were considerable flake debris, expanding to the edge of the worn crack. At this time, the wear mechanism was fatigue wear. During the friction process, the micro convex on the LR surface was subjected to the repeated load pulse of Si_3N_4 ceramic ball. When the LR sample was contacting with the ceramic ball surface, the actual contact points were discontinuous, and the micro convex on the two surfaces was colliding with each other to generate the impact force, thus making the micro convex subject to repeated impact and deformation, which caused the fatigue wear of the material.

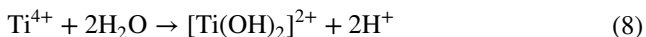
On the PN + PECVD sample, the depth of the worn crack was shallow, while a very tiny dent appeared in the worn crack. A few fine particles existed in the worn crack. In this scenario, the wear mechanism was abrasive wear. During the friction and wear processes, the film of PN + PECVD sample exhibiting high hardness on the surface fell off and turned out to be wear debris. The normal load on the grinding ball pressed the wear debris into the friction surface to form three-body wear. With the sliding of the grinding ball, wear debris furrowed on the surface under radial force and longitudinal load, so grooves and furrows appeared.

3.5 Electrochemical Performance

The electrochemical performance of Ti6Al4V, LR sample and PN + PECVD sample was ascertained to analyze its anti-corrosion performance in human simulated fluid. The surface of the LR sample and Ti6Al4V sample were Ti–O compound, the primary corrosion reaction equations in SBF are expressed as:

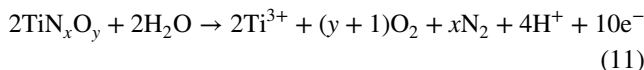
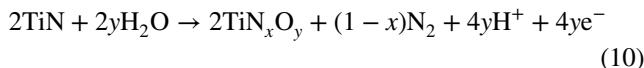


After the oxide film on the surface of Ti6Al4V was corroded, titanium in SBF primarily underwent the hydrolysis reaction. The main reaction equations are written as:



Yilbas et al. [25] investigated the corrosion state of Ti–N compounds in the SBF. The first corrosion referred to the

oxidation of TiN to form nitrogen oxides, while the secondary reaction was the re-oxidation of nitrogen oxides. The main reaction equations are defined as [26, 27]:



In the electrolyte, hydrogen evolution acted as a reduction reaction, and oxygen evolution referred to an oxidation reaction. Under the more negative electrode potential, the electron energy was higher. The electron would migrate from the electrode to the solution smoothly, and the easier hydrogen evolution would take place. Likewise, the more positive the electrode potential, the lower the electron energy would be, the more easily electrons would transfer from solution to electrode, and the easier oxygen evolution would occur. In other words, when the E_{corr} value was down-regulated, the corrosion tendency rose; when the E_{corr} value was up-regulated, the corrosion tendency declined. Figure 8 plots the electrochemical polarization curves of the three samples in the simulated body fluid. The corrosion potential of the sample after LR negative shifted by 0.048 V, while the corrosion potential of the PN + PECVD sample positive shifted by 0.038 V. The corrosion potential of PN + PECVD samples displayed a positive deviation, revealing that the compact compound formed on the surface of titanium alloy modified by PN + PECVD could effectively hinder the reaction between the corrosion solution and titanium alloy substrate. The LR sample displayed a negative shifted because of the enhancement of the surface roughness after remelting. The micro convex peaks formed on the surface hindered metal particles from escaping and produced partial discharge that caused pitting corrosion. Such factor would lead to more

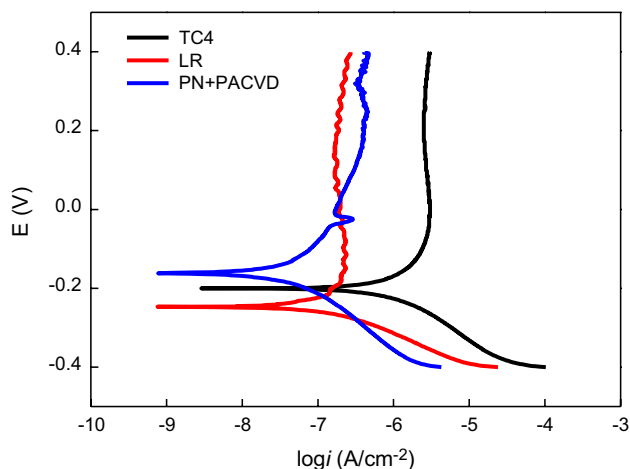


Fig. 8 Polarization curves of Ti6Al4V, LR and PN + PECVD sample

corrosion after LR, whereas the corrosion potential cannot act as a standard to determine the corrosion performance of metal materials [28, 29].

Given Faraday's law of electrolysis, mass can be associated with charge, as expressed in Eq. 12.

$$Q = nF \Delta m / M \quad (12)$$

where M denotes the molar mass of the metal; Δm represents the change in the mass of the metal during the reaction; n refers to the number of transferred charges in the corrosion reaction; F indicates the Faraday constant.

Assuming that the corrosion current density i_{corr} is constant within the time interval Δt , and the corrosion of the metal surface is absolutely uniform, the current can be integrated with the amount of electricity and time. Thus, Eq. 13 is yielded, where A denotes the electrode surface area,

$$i_{corr} = Q / A \Delta t \quad (13)$$

If the corrosion rate is considered the average depth of penetration of the material, the penetration rate ν can be expressed as:

$$\nu = i_{corr} M / nF \rho \quad (14)$$

where ρ denotes the metal density. From the above analysis, it is suggested that the corrosion rate was directly proportional to the corrosion current, so with the comparison of the corrosion current, the corrosion resistance of the three samples could be indirectly compared. The linear polarization method is usually adopted to calculate i_{corr} . A tiny potential $\Delta \eta$ is employed to E_{corr} to generate a tiny current Δi . Accordingly, the polarization resistance R_p can be obtained, and i_{corr} can be got by Eqs. 15 and 16.

$$R_p = \Delta \eta / \Delta i = \beta_a \beta_c / 2.303 i_{corr} (\beta_a + \beta_c) \quad (15)$$

i.e.

$$i_{corr} = \beta_a \beta_c / 2.303 R_p (\beta_a + \beta_c) \quad (16)$$

where β_a and β_c denote the tafel slopes of the anode and the cathode, respectively [30, 31].

According to the mentioned formula, the corrosion current of the three samples was calculated, as listed in Table 3. Corrosion current values followed the order of Ti6Al4V > LR > PN + PECVD. It is suggested that the composite process of PN + PECVD exhibited the optimal

corrosion resistance, followed by laser remelting modified samples, both of which were better than Ti6Al4V. The dense solid solution layer formed by Ti–N compounds on the surface and inside of PN + PECVD sample after modification was hard to react with the electrolyte in human body solution and exhibited prominent corrosion resistance. Though the corrosion voltage of LR sample was lower than that of Ti6Al4V, Ti–O-based compounds formed on LR sample surface could prevent the corrosion solution from entering the substrate, thereby effectively protecting the substrate.

4 Conclusions

In this paper, the anti-wear and anti-corrosion properties in SBF of Ti6Al4V modified by LR and PN + PECVD processes were studied, and the following conclusions are drawn: After LR and PN + PECVD modification, the microhardness of the sample surface was 840.33HV and 1024.41HV, 117% and 165% higher than that before the samples were modified, respectively. By the friction and wear experiments in simulated body fluid, the wear rate of LR and PN + PECVD samples was 5.65×10^{-5} and $1.20 \times 10^{-5} \text{ mm}^3/\text{N m}$, 74.1% and 94.5% lower than that of Ti6Al4V before the samples were modified, respectively. In the simulated body fluid, Ti6Al4V substrate followed the main wear mechanism of adhesive wear, LR sample complied with fatigue wear, and PN + PECVD sample followed abrasive wear. By the electrochemical corrosion experiment, the corrosion current of Ti6Al4V substrate, LR and PN + PECVD samples were obtained as 1.426×10^{-6} , 2.023×10^{-7} , $5.296 \times 10^{-8} \text{ A cm}^2$, respectively. The corrosion resistance followed the order of PN + PECVD > LR > Ti6Al4V.

LR and PN + PECVD modification processes can effectively improve the hardness, wear resistance and corrosion resistance of Ti6Al4V in SBF, which provides a theoretical and experimental basis for the promotion of the two processes in the surface strengthening of biological titanium alloys. However, this study still has certain limitations. For example, the antibacterial properties of implants and in vivo cell diffusion tests have not been studied, and further research are needed.

Table 3 Polarization parameters of Ti6Al4V, LR and PN + PECVD sample

Sample	E _{corr} /V	I _{corr} /A cm ²	β _c /V decade ⁻¹	β _a /V decade ⁻¹	R _p /Ω cm ²
Ti6Al4V	-0.201	1.426 × 10 ⁻⁶	7.795	3.029	28,173
LR sample	-0.249	2.023 × 10 ⁻⁷	11.651	0.950	170,546
PN + PECVD sample	-0.163	5.296 × 10 ⁻⁸	7.283	4.584	691,780

Acknowledgements This project were supported by the Fundamental Research Funds for the Central Universities (Grant No. 2232018A3-08) and (Grant No. 2232018D3-04).

Compliance with Ethical Standards

Conflict of interest The authors declare that they have no known competing financial interests or personal relationships that could have appeared to influence the work reported in this paper.

References

1. M. Geetha, A.K. Singh, R. Asokamani, A.K. Gogia, *Prog. Mater. Sci.* **54**, 397 (2009)
2. I. Cvijović-Alagić, Z. Cvijović, S. Mitrović, V. Panić, *Corros. Sci.* **53**, 796–802 (2011)
3. R.S. Flatebo, A.C. Johannessen, A.G. Grønningsaeter, O.E. BoE, N.R. Gjerdet, B. Grung, K.N. Leknes, *J. Period.* **77**, 1201 (2006)
4. S.R. Thomas, D. Shukla, *Latham PD Bone Joint J.* **86**, 974 (2004)
5. R.I.M. Asri, W.S.W. Harun, M. Samykano, N.A.C. Lah, S.A.C. Ghani, F. Tarlochan, *Mater. Sci. Eng.* **77**, 1261 (2017)
6. D. Park, Y.H. Kim, J.K. Lee, *J. Mater. Sci.* **38**, 4933 (2003)
7. M.A. Farid, A. Amir, A. Mohammad, *Wear* **390–391**, 93 (2017)
8. A. Borrás, A. Barranco, A.R. González-Elípe, *J. Mater. Sci.* **41**, 5220 (2006)
9. J. Ding, J. Hao, Q. Xue, W. Liu, *J. Mater. Sci.* **43**, 645 (2008)
10. P. Mina, A. Mahboobeh, A. Shahrokh, *Surf. Coat. Technol.* **366**, 366 (2019)
11. G. Hamed, A.Z. Amir, B. Fatemeh, P. Abbas, *Appl. Surf. Sci.* **456**, 402 (2018)
12. C. Mitterer, F. Holler, D. Reitberger, *Surf. Coat. Technol.* **163**, 716 (2003)
13. W. Ge, Z. Chang, A. Siddique, C. Liu, *Ceram. Int.* **46**, 7355 (2020)
14. V. Chawla, R. Jayaganthan, R. Chandra, *Mater. Charact.* **59**, 1015 (2008)
15. Y. Chen, L. Song, C. Zhang, X. Ye, J. Hu, *Vac.* **143**, 98 (2017)
16. J. Morgiel, K. Szymkiewicz, Ł. Maja, M. Tarnowski, T. Wierzchoń, *Surf. Coat. Technol.* **359**, 183 (2019)
17. J. Sun, Q.T. Yao, Y.H. Zhang, X.D. Du, Y.C. Wu, W.P. Tong, *Surf. Coat. Technol.* **309**, 382 (2017)
18. F. Zhang, M. Yan, J. He, F.X. Yin, *Vacuum* **142**, 106 (2017)
19. S.R. Hosseini, A. Ahmadi, *Vac.* **87**, 30 (2013)
20. O. Durst, J. Ellermeier, C. Berger, *Surf. Coat. Technol.* **203**, 848 (2008)
21. K.V.S. Srinadh, V. Singh, *Bull. Mater. Sci.* **27**, 347 (2004)
22. C. Leyens, M. Peters, W.A. Kaysser, *Mater. Sci. Technol.* **12**, 213 (1996)
23. T. Zhang, Q. Fan, X.L. Ma, W. Wang, K.S. Wang, P.Q. Shen, J.L. Yang, L.Q. Wang, *Mater. Lett.* **253**, 310 (2019)
24. S. Taktak, H. Akbulut, *Vac.* **75**, 247 (2004)
25. B.S. Yilbas, A.Z. Sahin, Z. Ahmad, B.J. Abdul Aleem, *Corros. Sci.* **37**, 1627 (1995)
26. V.M.C.A. Oliveira, C. Aguiar, A.M. Vazquez, A. Robin, J.M.R. Barboza, *Corros. Sci.* **88**, 317 (2014)
27. M. Atapour, A.L. Pilchak, G.S. Frankel, J.C. Williams, *Mater. Sci. Eng. C* **31**, 885 (2011)
28. A. Ghanbari, H. Jafari, F. Ashenai Ghasemi, *Met. Mater. Int.* **26**, 395 (2020)
29. C. Wenfang, N. Fengjuan, T. Yun-ling, G.W. Qin, *T Nonferr. Metal. Soc.* **29**, 1026 (2019)
30. M.S. Ahmed, P. Munroe, Z.T. Jiang, *Corros. Sci.* **53**, 3678 (2011)
31. M.A. Farid, A. Amir, A. Mahmood, A. Mohammad, *Wear* **390**, 93 (2017)

Publisher's Note Springer Nature remains neutral with regard to jurisdictional claims in published maps and institutional affiliations.